We are IntechOpen, the world's leading publisher of Open Access books
Built by scientists, for scientists

6,900
Open access books available

185,000
International authors and editors

200M
Downloads

154
Countries delivered to

Our authors are among the

TOP 1%
most cited scientists

12.2%
Contributors from top 500 universities

BOOK CITATION INDEX
CLARIVATE ANALYTICS
INDEXED

WEB OF SCIENCE™

Selection of our books indexed in the Book Citation Index
in Web of Science™ Core Collection (BKCI)

Interested in publishing with us?
Contact book.department@intechopen.com

Numbers displayed above are based on latest data collected.
For more information visit www.intechopen.com

Operational Amplifiers and Active Filters: A Bond Graph Approach

Gilberto González and Roberto Tapia
University of Michoacan
Mexico

1. Introduction

The most important single linear integrated circuit is the operational amplifier. Operational amplifiers (op-amp) are available as inexpensive circuit modules, and they are capable of performing a wide variety of linear and nonlinear signal processing functions (Stanley, 1994).

In simple cases, where the interest is the configuration gain, the ideal op-amp in linear circuits, is used. However, the frequency response and transient response of operational amplifiers using a dynamic model can be obtained.

The bond graph methodology is a way to get an op-amp model with important parameters to know the performance. A bond graph is an abstract representation of a system where a collection of components interact with each other through energy ports and are place in the system where energy is exchanged (Karnopp & Rosenberg, 1975).

Bond graph modelling is largely employed nowadays, and new techniques for structural analysis, model reduction as well as a certain number of software packages using bond graph have been developed.

In (Gawthrop & Lorcan, 1996) an ideal operational amplifier model using the bond graph technique has been given. This model only considers the open loop voltage gain and show an application of active bonds.

In (Gawthrop & Palmer, 2003), the `virtual earth' concept has a natural bicausal bond graph interpretation, leading to simplified and intuitive models of systems containing active analogue electronic circuits. However, this approach does not take account the type of the op-amp to consider their internal parameters.

In this work, a bond graph model of an op-amp to obtain the time and frequency responses is proposed. The input and output resistances, the open loop voltage gain, the slew rate and the supply voltages of the operational amplifier are the internal parameters of the proposed bond graph model.

In the develop of this work, the Bond Graph model in an Integral causality assignment (BGI) to determine the properties of the state variables of a system is used (Wellstead, 1979; Sueur & Dauphin-Tanguy, 1991). Also, the symbolic determination of the steady state of the variables of a system based on the Bond Graph model in a Derivative causality assignment (BGD) is applied (Gonzalez et al., 2005). Finally, the simulations of the systems represented

by bond graph models using the software 20-Sim by Controllab Products are realized (Controllab Products, 2007).

Therefore, the main result of this work is to present a bond graph model of an op-amp considering the internal parameters of a type of linear integrated circuit and external elements connected to the op-amp, for example, the feedback circuit and the load.

The outline of the paper is as follows. Section 2 and 3 summarizes the background of bond graph modelling with an integral and derivative causality assignment. Section 4 the bond graph model of an operational amplifier is proposed. Also, the frequency responses of the some linear integrated circuits that represent operational amplifier using the proposed bond graph model are obtained. Section 5 gives a comparator circuit using a bond graph model and obtaining the time response. Section 6 presents the proposed bond graph model of an feedback op-amp; the input and output resistances, bandwidth, slew rate and supply voltages of a non-inverting amplifier using BGI and BGD are determined. Section 7 gives the filters using a bond graph model of an op-amp. In this section, we apply the filters for a complex signal in the physical domain. The bond graph model of an op-amp to design a Proportional and Integral (PI) controller and to control the velocity of a DC motor in a closed loop system is applied in section 8. Finally, the conclusions are given in section 9.

2. Bond graph model

Consider the following scheme of a Bond Graph model with an Integral causality assignment (BGI) for a multiport Linear Time Invariant (LTI) system which includes the key vectors of Fig. 1 (Wellstead, 1979; Sueur & Dauphin-Tanguy, 1991).
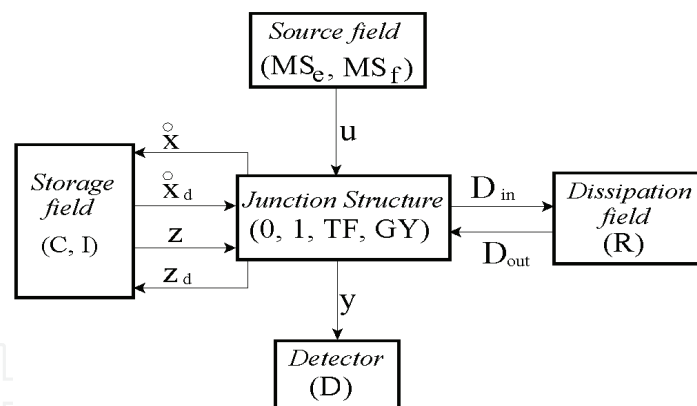

Fig. 1. Key vectors of a bond graph.

In fig. 1, $\left(MS_e, MS_f \right)$, $\left(C, I \right)$ and $\left(R \right)$ denote the source, the energy storage and the energy dissipation fields, $\left(D \right)$ the detector and $\left(0, 1, TF, GY \right)$ the junction structure with transformers, TF, and gyrators, GY.

The state $x(t) \in \mathfrak{R}^n$ and $x_d(t) \in \mathfrak{R}^m$ are composed of energy variables $p(t)$ and $q(t)$ associated with I and C elements in integral causality and derivative causality, respectively, $u(t) \in \mathfrak{R}^p$ denotes the plant input, $y(t) \in \mathfrak{R}^q$ the plant output, $z(t) \in \mathfrak{R}^n$ the co-energy vector, $z_d(t) \in \mathfrak{R}^m$ the derivative co-energy and $D_{in}(t) \in \mathfrak{R}^r$ and $D_{out}(t) \in \mathfrak{R}^r$ are a mixture

of $e(t)$ and $f(t)$ showing the energy exchanges between the dissipation field and the junction structure (Wellstead, 1979; Sueur & Dauphin-Tanguy, 1991).
The relations of the storage and dissipation fields are,

$$z(t) = Fx(t) \tag{1}$$

$$z_d(t) = F_d x_d(t) \tag{2}$$

$$D_{out}(t) = LD_{in}(t) \tag{3}$$

The relations of the junction structure are,

$$\begin{bmatrix} \dot{x}(t) \\ D_{in}(t) \\ y(t) \end{bmatrix} = \begin{bmatrix} S_{11} & S_{12} & S_{13} & S_{14} \\ S_{21} & S_{22} & S_{23} & 0 \\ S_{31} & S_{32} & S_{33} & 0 \end{bmatrix} \begin{bmatrix} x(t) \\ D_{out}(t) \\ u(t) \\ \dot{x}_d(t) \end{bmatrix} \tag{4}$$

$$z_d(t) = -S_{14}^T z(t) \tag{5}$$

The entries of S take values inside the set $\{0, \pm 1, \pm m, \pm n\}$ where m and n are transformer and gyrator modules; S_{11} and S_{22} are square skew-symmetric matrices and S_{12} and S_{21} are matrices each other negative transpose. The state equation is (Wellstead, 1979; Sueur & Dauphin-Tanguy, 1991),

$$\dot{x}(t) = A_p x(t) + B_p u(t) \tag{6}$$

$$y(t) = C_p x(t) + D_p u(t) \tag{7}$$

where

$$A_p = E^{-1}(S_{11} + S_{12} M S_{21})F \tag{8}$$

$$B_p = E^{-1}(S_{13} + S_{12} M S_{23}) \tag{9}$$

$$C_p = (S_{31} + S_{32} M S_{21})F \tag{10}$$

$$D_p = S_{33} + S_{32} M S_{23} \tag{11}$$

being

$$E = I_n + S_{14} F_d^{-1} S_{14}^T F \tag{12}$$

$$M = \left(I_n - LS_{22} \right)^{-1} L \tag{13}$$

3. Bond graph in derivative causality assignment

We can use the Bond Graph in Derivative causality assignment (BGD) to solve directly the problem to get A_p^{-1}. Suppose that A_p is invertible and a derivative causality assignment is performed on the bond graph model (Gonzalez et al., 2005). From (4) the junction structure is given by,

$$\begin{bmatrix} z(t) \\ D_{ind}(t) \\ y_d(t) \end{bmatrix} = \begin{bmatrix} J_{11} & J_{12} & J_{13} \\ J_{21} & J_{22} & J_{23} \\ J_{31} & J_{32} & J_{33} \end{bmatrix} \begin{bmatrix} \dot{x}(t) \\ D_{outd}(t) \\ u(t) \end{bmatrix} \tag{14}$$

where the entries of J have the same properties that S and the storage elements in (14) have a derivative causality. Also, D_{ind} and D_{outd} are defined by

$$D_{outd}(t) = L_d D_{ind}(t) \tag{15}$$

and they depend of the causality assignment for the storage elements and that junctions have a correct causality assignment.

From (6) to (13) and (14) we obtain,

$$z(t) = A_p^* \dot{x}(t) + B_p^* u(t) \tag{16}$$

$$y_d(t) = C_p^* \dot{x}(t) + D_p^* u(t) \tag{17}$$

where

$$A_p^* = J_{11} + J_{12} N J_{21} \tag{18}$$

$$B_p^* = J_{13} + J_{12} N J_{23} \tag{19}$$

$$C_p^* = J_{31} + J_{32} N J_{21} \tag{20}$$

$$D_p^* = J_{33} + J_{32} N J_{23} \tag{21}$$

being

$$N = \left(I_n - L_d J_{22} \right)^{-1} L_d \tag{22}$$

The state output equations of this system in integral causality are given by (6) and (7). It follows, from (1), (6), (7), (16) and (17) that,

$$A_p^* = FA_p^{-1} \tag{23}$$

$$B_p^* = -FA_p^{-1}B_p \tag{24}$$

$$C_p^* = C_pA_p^{-1} \tag{25}$$

$$D_p^* = D_p - C_pA_p^{-1}B_p \tag{26}$$

Considering $\dot{x}(t) = 0$, the steady state of a LTI MIMO system defined by

$$x_{ss} = -A_p^{-1}B_pu_{ss} \tag{27}$$

$$y_{ss} = \left(D_p - C_pA_p^{-1}B_p\right)u_{ss} \tag{28}$$

where x_{ss} and y_{ss} are the steady state of the state variables and the output, respectively.
In an approach of the BGD, the steady state is determined by

$$x_{ss} = F^{-1}B_p^*u_{ss} \tag{29}$$

$$y_{ss} = D_p^*u_{ss} \tag{30}$$

4. A bond graph model of an operational amplifier

The standard operational amplifier (op-amp) symbol is shown in Fig. 2. It has two input terminals, the inverting (-) input and the noninverting (+) input, and one output terminal. The typical op-amp operates with two Direct Current (DC) supply voltages, one positive and the other negative (Stanley, 1994).
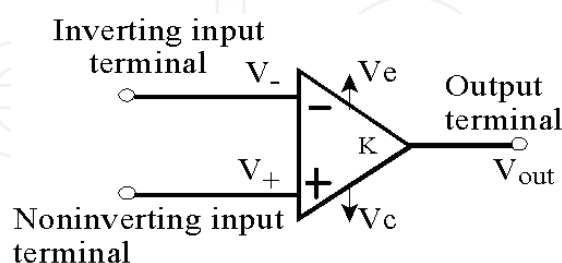

Fig. 2. Operational amplifier symbol.

The complex action of the op-amp results in the amplification of the difference between the voltages at the noninverting, V_+, and the inverting, V_-, inputs by a large gain factor, K, designed open loop gain. The output voltage is,

$$V_{out} = K\left(V_+ - V_-\right) \tag{31}$$

The assumptions of the ideal op-amp are (Barna & Porat, 1989): 1) The input impedance is infinite. 2) The output impedance is zero. 3) The open loop gain is infinite. 4) Infinite bandwidth so that any frequency signal from 0 to ∞ Hz can be amplified without attenuation. 5) Infinite slew rate so that output voltage charges simultaneously with input voltage charges.

The implications of the assumptions are: no current will flow either into or out of either input terminal of the op-amp, also, the voltage at the output terminal does not charge as the loading is varied and finally, from H_3, $V_+ - V_- = \dfrac{V_{out}}{K}$, if we take the limit when K→∞, note that $V_+ = V_-$, which indicates that the voltages at the two input terminals are forced to be equal in the limit.

The assumptions of an op-amp are not completely true in practice, and to be fully competent in the analysis and design of op-amps circuits, one must be aware of the limitations. Therefore, we propose a more realistic model applicable to DC and low frequencies based on Bond Graph with Intregral causality assignment (BGI), since an op-amp is a multistage amplifier, it can be represented by Fig. 3.
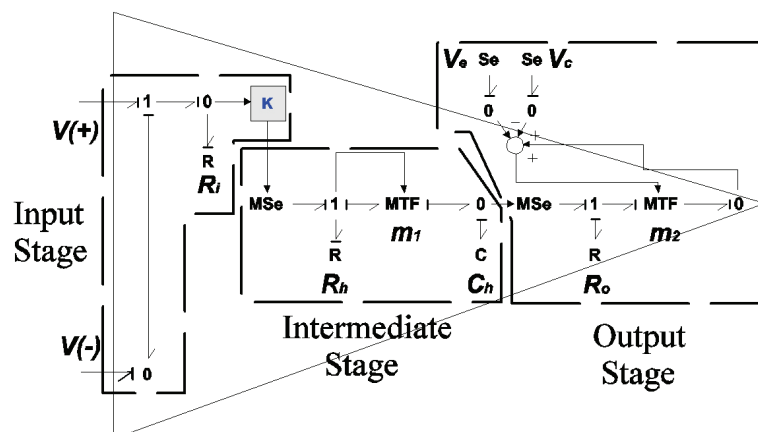

Fig. 3. Bond graph model of an operational amplifier.

The individual stages used in op-amp are separately chosen to develop different amplifier characteristics. Those amplifier characteristics which are determined by a given stage depend on whether it functions as an input stage, intermediate stage or output stage. So, the bond graph model of the op-amp is composed by 3 stages, which are:

- Characteristics of the differential input stage of an operational amplifier are the most critical factors which affect the accuracy of an op-amp in providing voltage gain. Errors effects of following stages are reduced in significance by the gain isolation provided by the first stage. This input stage considers the two input terminals of op-amp, the differential input resistance, denoted as R_i, which is the resistance between the inverting and non-inverting inputs and K is the open loop gain.
- The intermediate stage introduces the frequency compensation of the op-amp using a lag network. Also, using a MTF, the slew rate of the op-amp is considered.
- Following the input and intermediate voltage gain stages of an op-amp, it is desirable to provide impedance isolation from loads. In this way the characteristics of the gain

stages are preserved under load, and adequate signal current is made available to the load. In addition, the output stage provides isolation to the preceding stage and a low output impedance to the load. This stage is formed by the output terminal, the output resistance of the op-amp denoted as R_o and the adjustment of supply voltages, positive voltage V_c and negative voltage V_e, are applied using a MTF element.

The usefulness of the bond graph model of an operational amplifier can be shown, applying this model to $\mu A741$ op-amp by Fairchild Semiconductor Corporation (Stanley, 1994; Gayakward, 2000) and, $TL084$ and $OP27$ by Texas Instruments (Stanley, 1994; Gayakward, 2000) whose data sheets are shown in Table 1.

Op-amp	$\mu A741$	$TL084$	$OP27$
$R_i(\Omega)$	2×10^6	10^{12}	6×10^6
$R_o(\Omega)$	75	75	70
K	2×10^5	2×10^5	1.8×10^6
$SR(V/\mu s)$	0.5	13	2.8
$V_c, V_e(V)$	± 15	± 18	± 22

Table 1. Data sheets of $\mu A741$, $TL084$ and $OP27$.

Using the data sheets of an op-amp, the high cutoff frequency of the open loop voltage gain, f_o, is determined. Moreover, the compensation parameters of the bond graph model are defined by

$$f_o = \frac{1}{2\pi R_c C_c} \tag{32}$$

From (32) and the data sheets of the $\mu A741$, $TL084$ and $OP27$ op-amps, the parameters to obtain the frequency response are given in Table 2.

Op-amp	$\mu A741$	$TL084$	$OP27$
$R_h(\Omega)$	10^3	10^3	10^3
$C_h(F)$	3.06652×10^{-6}	5.3051×10^{-6}	1.9894×10^{-5}

Table 2. Parameters of frequency response.

Substituting the parameters of Tables 1 and 2 to bond graph model of each op-amp, the frequency responses of $\mu A741$, $TL084$ and $OP27$ op-amps are shown in Fig. 4, 5 and 6, respectively.

Note that, the frequency responses of the $\mu A741$, $TL084$ and $OP27$ op-amps are very close respect to the data sheets of these op-amps (Stanley, 1994; Gayakward, 2000). Also, decibel gain is $K_{dB} = 20Log(K)$. The next section an application of the bond graph model of an op-amp to prove the time response is presented.
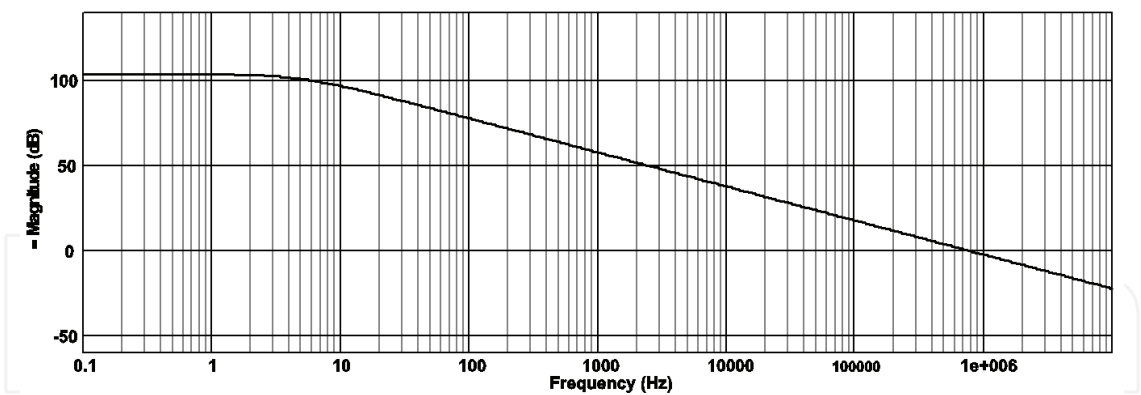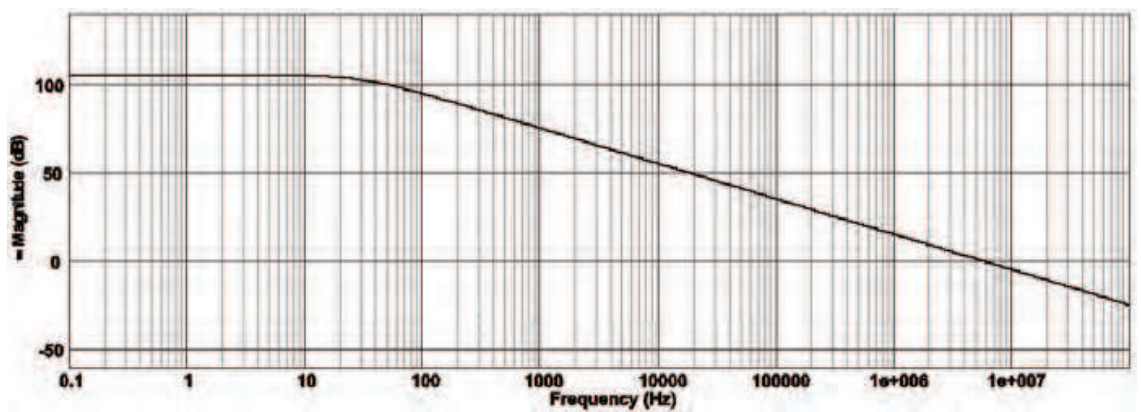
Fig. 4. Frequency response of $\mu A741$ op-amp.

Fig. 5. Frequency response of $TL084$ op-amp.
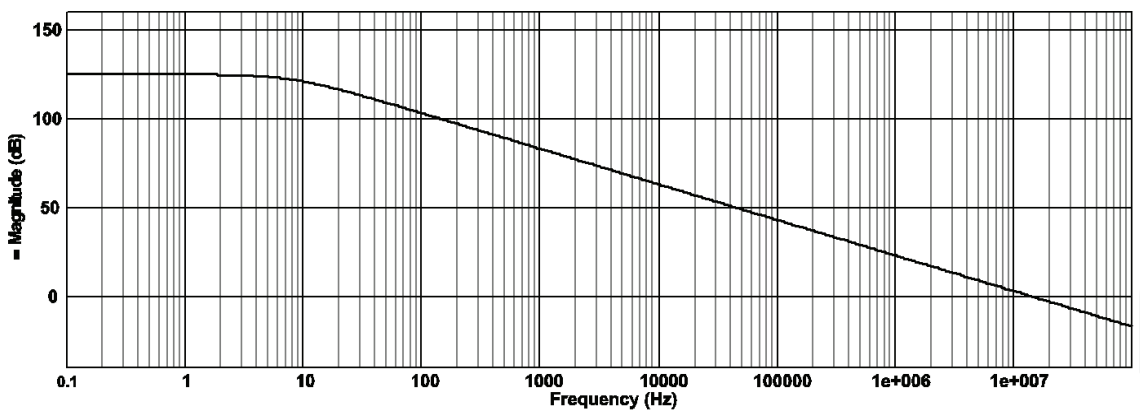
Fig. 6. Frequency response of $OP27$ op-amp.

5. Comparator circuit

Comparator circuits represent to the first class of circuits we have considered that are basically nonlinear in operation. Specifically, comparator circuits produce two or more discrete outputs, each of which is dependent on the input level (Floyd & Buchla, 1999). In this application, the op-amp is used in the open loop configuration with the input voltage on one input and a reference voltage on the other, which is shown in Fig. 7.

Fig. 7. Bond graph model of a comparator op-amp.

Applying a voltage $v_+(t) = 3\sin(2\pi f_+ t)V$ to the noninverting input, where $f_+ = 0.15Hz$ and $v_- = 1V$ to the inverting input of the bond graph model of Fig. 7. Also, the supply voltages are $V_c = 12V$ and $V_e = -12V$, the time response of the comparator circuit using the $\mu A741$ op-amp is shown in Fig. 8.

Fig. 8. Time response of the comparator op-amp.

In according with the objective of the comparator circuit, the time response of the Fig. 8 is satisfactory (Stanley, 1994; Gayakward, 2000; Floyd & Buchla, 1999). However, if the frequency of the input signal increases, we have to consider the response of phase shift versus frequency, which is obtained using the proposed bond graph model and is shown in Fig. 9 for $\mu A741$ op-amp phase shift between the input and output signals.

If the noninverting input voltage is $v_+(t) = 0.1\sin(2\pi f_+ t)V$ where $f_+ = 100Hz$, the inverting input voltage is $v_-(t) = 0V$ and, the supply voltages are $V_c = 12V$ and

$V_e = -12V$, then the time response of the comparator circuit using $\mu A741$ op-amp is a square waveform of magnitude $\pm 12V$ and a phase shift of $\theta = -86.8^0$ respect the input signal, which is shown in Fig. 10.
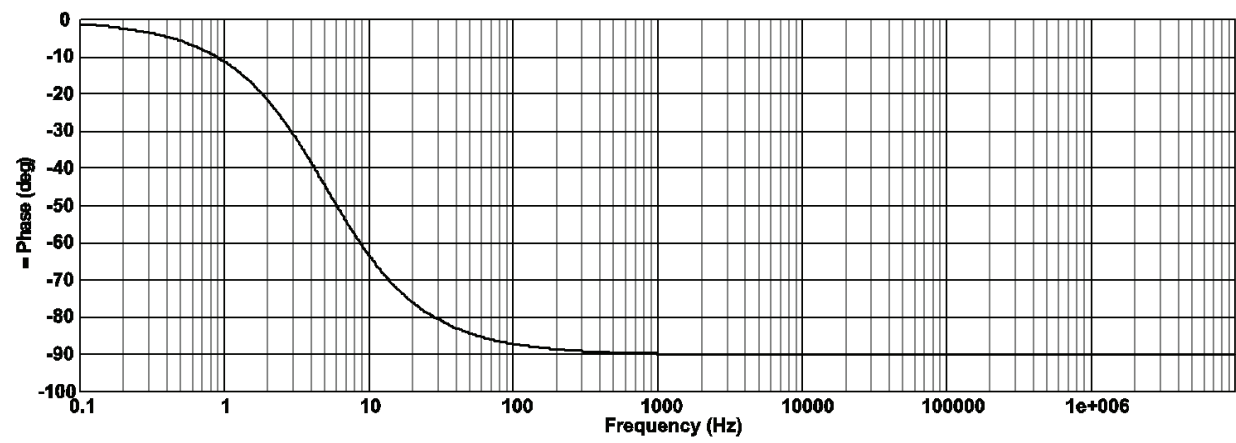

Fig. 9. Phase shift versus frequency of $\mu A741$ op-amp.
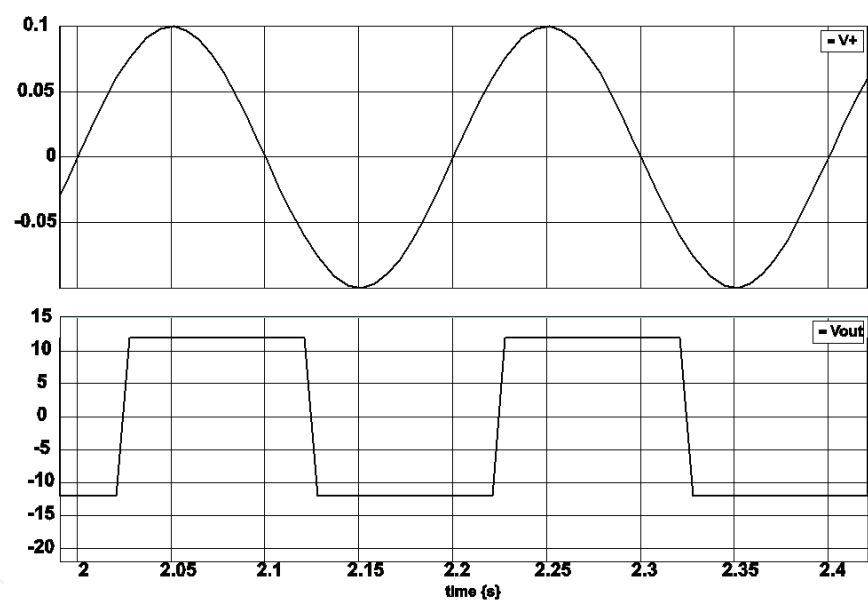

Fig. 10. Time response of comparator with $V_+(t) = 20\sin(200\pi t)$.

The phase shift of the output signal of Fig. 10 can be verified from the following equation, calculating the lag time of the output signal,

$$t = \frac{\theta}{360 f} \tag{33}$$

where θ is the phase shift of the bode plot for $\mu A741$ op-amp is the Fig. 8, and f is the frequency of the input signal. In this case $t = 2.41ms$.

In next section op-amp configurations with negative feedback in the physical domain are proposed.

6. Feedback operational amplifier

An op-amp that uses feedback is called a feedback is called a feedback amplifier. A feedback amplifier is sometimes referred to as a closed loop amplifier because the feedback forms a closed loop between the input and the output. A feedback amplifier essentially consists of two parts: an op-amp and a feedback circuit. The feedback circuit can take any form whatsoever, depending on the intended application of the amplifier. This means that the feedback circuit may be made up of either passive components, active components, or combinations of both (Gayakward, 2000).

A closed loop amplifier can be represented by using two blocks, one for an op-amp and another for a feedback circuit. There are four ways to connect theses two blocks. These connections are classified according to whether the voltage or current is fed back to the input in series or in parallel, as follows: 1) Voltage series feedback, 2) Voltage shunt feedback, 3) Current series feedback and 4) Current shunt feedback (Gayakward, 2000) and (Floyd & Buchla, 1999).

The voltage series feedback configuration is one of the most important because this is commonly used. An in depth analysis of this configuration in the physical domain is presented in this section, computing voltage gain, input resistance, output resistance and the bandwidth.

6.1 A bond graph model of a noninverting amplifier

An op-amp connected in a closed loop configuration as a noninverting amplifier is shown in Fig. 11. The input signal is applied to the noninverting input. A portion of the output is applied back to the inverting input through the feedback network in the physical domain. The BGI and the Bond Graph in a Derivative causality assignment (BGD) are shown in Fig. 11, in order to get the symbolic expressions of the closed loop system in steady state applying the methodology given in section 1.
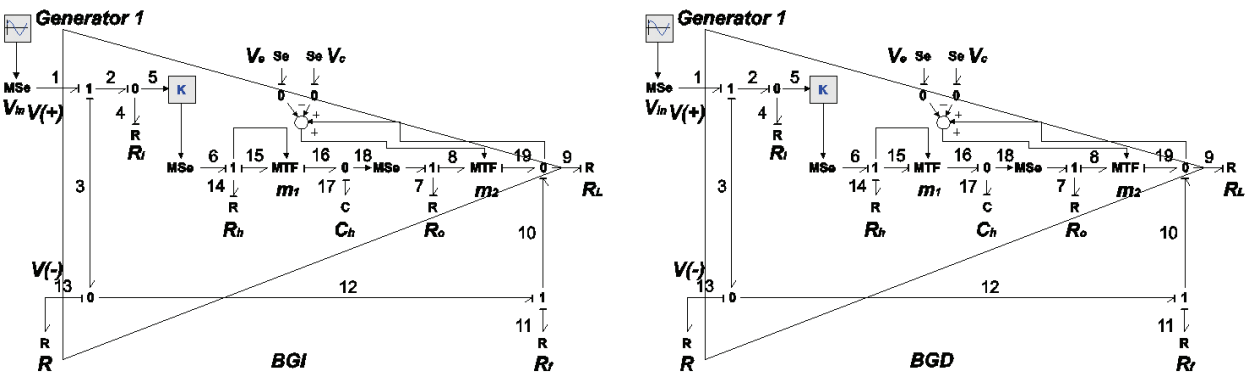

Fig. 11. Bond graph models of a noninverting amplifier.

The closed loop gain, A_{CL}, can be determined using the BGD approach, from (30) we have,

$$A_{CL} = \frac{y_{ss}}{u_{ss}} = D_p^*$$

(34)

where y_{ss} and u_{ss} are the steady state values of the output and input, respectively.

We now derive the closed loop gain of the noninverting amplifier using the BGD. The key vectors of BGD are given by,

$$
\begin{aligned}
&x(t) = q_{17}(t); \dot{x}(t) = f_{17}(t); z(t) = e_{17}(t)\\
&u(t) = e_1(t); y(t) = e_9(t)\\
&D_{ind}(t) = \begin{bmatrix} e_4(t) & e_7(t) & e_9(t) & f_{11}(t) & f_{13}(t) & f_{14}(t) \end{bmatrix}\\
&D_{outd}(t) = \begin{bmatrix} f_4(t) & f_7(t) & f_9(t) & e_{11}(t) & e_{13}(t) & e_{14}(t) \end{bmatrix}
\end{aligned}
\tag{35}
$$

the constitutive relations are,

$$
F = \frac{1}{C_h}
\tag{36}
$$

$$
L_d = diag \left\{ \frac{1}{R_i}, \frac{1}{R_o}, R_F, R, R_h \right\}
\tag{37}
$$

and the junction structure is,

$$
J_{21} = \begin{bmatrix} 0 \\ 0 \\ 0 \\ 0 \\ 0 \\ \dfrac{1}{m} \end{bmatrix}; J_{22} = \begin{bmatrix} 0 & 0 & 0 & 0 & -1 & 0 \\ 0 & 0 & 0 & m_2 & \dfrac{-K}{m_1} - m_2 & \dfrac{-1}{m_1} \\ 0 & 0 & 0 & -1 & 1 & 0 \\ 0 & -m & 1 & 0 & 0 & 0 \\ 1 & m_2 & -1 & 0 & 0 & 0 \\ 0 & 0 & 0 & 0 & 0 & 0 \end{bmatrix}; J_{23} = \begin{bmatrix} 1 \\ \dfrac{K}{m_1} \\ 0 \\ 0 \\ 0 \\ 0 \end{bmatrix}
$$

$$
J_{12} = \begin{bmatrix} 0 & 0 & 0 & 0 & \dfrac{-K}{m_1} & \dfrac{-1}{m_1} \end{bmatrix}; J_{32} = \begin{bmatrix} 0 & 0 & 0 & -1 & 1 & 0 \end{bmatrix}
\tag{38}
$$

$$
J_{13} = \frac{K}{m_1}; J_{11} = J_{31} = J_{33} = 0
$$

From (21), (22), (34), (36), (37) and (38), the closed loop gain of the noninverting amplifier is,

$$
A_{CL} = \frac{R_L \left[m_2 R_i K (R + R_f) + m_1 R R_o \right]}{m_1 R_o \Delta + K R m_2 R_L R_i + R_L m_2^2 m_1 \left[R_f (R + R_i) + R R_i \right]}
\tag{39}
$$

where $\Delta = (R + R_i)(R_L + R_f) + R R_i$

Note that the closed loop gain (39) takes account the internal parameters and the external elements connected to op-amp.

A normal operation of the op-amp using the bond graph model indicates the modules of $MTF's$ are $m_1 = 1$, the slew rate is sufficient of the op-amp, and $m_2 = 1$, the supply voltages allow to obtain the output voltage depending the input voltage and the gain of the op-amp. Considering, $m_1 = 1$, $m_2 = 1$ and $R_o = 0$, we obtain

$$(A_{CL})_1 = \frac{R + R_f}{R + \frac{1}{K}\left(R_f + RR_i + \frac{R_f R}{R_i}\right)} \tag{40}$$

Applying the $\underset{\substack{R_i \to \infty \\ K \to \infty}}{Lim}(A_{CL})_1$, the ideal closed loop gain of this amplifier, $(A_{CL})_i$, is determined,

$$(A_{CL})_i = 1 + \frac{R_f}{R} \tag{41}$$

The time response of the noninverting amplifier using $\mu A741$ op-amp, $R = 10K\Omega$, $R = 190K\Omega$ and the input signal is $v_i(t) = 0.5\sin(2\pi f_i t)V$ where $f_i = 1KHz$, is shown in Fig. 12.
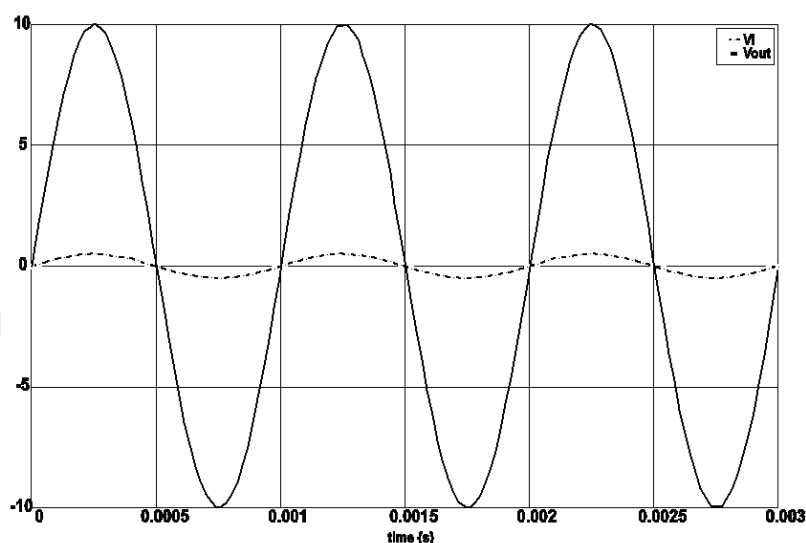

Fig. 12. Time response of the noninverting amplifier.

6.1.1 Input resistance of the noninverting amplifier

The input resistance of the noninverting amplifier can be determined using the BGD of Fig. 11. Considering the output $f_1(t)$, the submatrices J_{31}, J_{32} and J_{33} from (38) are changed by

$$J_{23} = \begin{bmatrix} 1 & 0 & 0 & 0 & 0 & 0 \end{bmatrix}; J_{13} = J_{33} = 0 \qquad (42)$$

From (21), (22), (37) and (38) the input resistance is determined by,

$$R_{iF} = \frac{R_o\left[(R+R_i)(R_L+R_f)+RR_i\right]+KRR_LR_i+R_L\left[R_f(R+R_i)+RR_i\right]}{(R+R_f)(R_o+R_L)+R_oR_L} \qquad (43)$$

where $(e_1)_{ss}$ and $(f_1)_{ss}$ are the steady state values of the input e_1 and output f_1, respectively. If $R_o = 0$ we reduce,

$$(R_{iF})_1 = R_i\left(1+\frac{KR}{R+R_f}\right)+\frac{RR_f}{R+R_f} \qquad (44)$$

finally, the term $\dfrac{R_fR}{R+R_f} \ \square \ R_i\dfrac{KR}{R+R_f}$ hence the ideal input resistance of the noninverting amplifier $(R_{iF})_i$ is defined by,

$$(R_{iF})_i = R_i\left(1+\frac{KR}{R+R_f}\right) \qquad (45)$$

The result of (45) indicates that the ideal input resistance of the op-amp with feedback is $(1+KR/R+R_f)$ times that without feedback. In addition, the equation (43) allows to determine the input resistance of the op-amp considering the internal parameters and external elements for this configuration. Equation (45) can be verified in (Stanley, 1994; Gayakward, 2000).

6.1.2 Output resistance of the noninverting amplifier
Output resistance is the resistance determined looking back into the feedback amplifier from the output terminal. A BGD that allows to obtain the output resistance of a noninverting amplifier is shown in Fig. 13.
The key vectors of the BGD of Fig. 13 are,

$$
\begin{aligned}
&x(t) = q_{16}(t); \dot{x}(t) = f_{16}(t); z(t) = e_{16}(t) \\
&u(t) = e_1(t); y(t) = f_1(t) \\
&D_{ind}(t) = \begin{bmatrix} e_4(t) & e_7(t) & e_{10}(t) & f_{12}(t) & e_{13}(t) \end{bmatrix} \\
&D_{outd}(t) = \begin{bmatrix} f_4(t) & f_7(t) & f_{10}(t) & e_{12}(t) & f_{13}(t) \end{bmatrix}
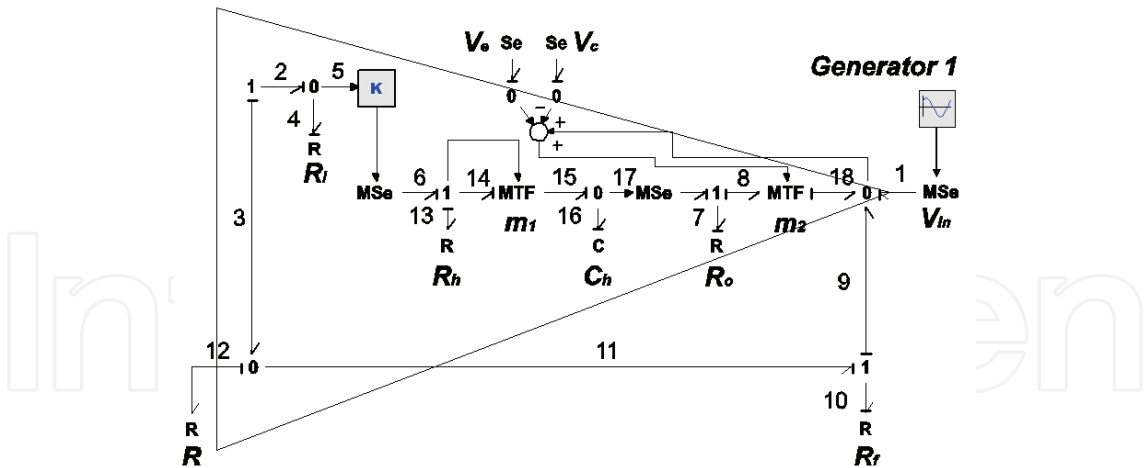\end{aligned}
\qquad (46)
$$

Fig. 13. Derivation of output resistance of a bond graph model of a noninverting amplifier.

the constitutive relations are,

$$L = diag\left\{\frac{1}{R_i}, \frac{1}{R_o}, \frac{1}{R_f}, R, \frac{1}{R_h}\right\}$$ (47)

$$F = \frac{1}{C_h}$$ (48)

and the junction structure of the BGD is,

$$J_{22} = \begin{bmatrix} 0 & 0 & 0 & -1 & 0 \\ 0 & 0 & 0 & K & -1 \\ 0 & 0 & 0 & 1 & 0 \\ 1 & 0 & -1 & 0 & 0 \\ 0 & 0 & 0 & 0 & 0 \end{bmatrix}; J_{21} = \begin{bmatrix} 0 \\ 0 \\ 0 \\ 0 \\ 1 \end{bmatrix}; J_{21} = J_{32}^T = \begin{bmatrix} 0 \\ -1 \\ -1 \\ 0 \\ 0 \end{bmatrix}$$ (49)

$$J_{12} = \begin{bmatrix} 0 & 0 & 0 & -K & -1 \end{bmatrix}; J_{11} = J_{13} = J_{31} = J_{33} = 0$$

Substituting (22), (47), (49) into (21) the output resistance of a noninverting amplifier is obtained,

$$R_{oF} = \frac{(e_1)_{ss}}{(f_1)_{ss}} = \left(D_p^*\right)^{-1} = \frac{R_o\left[R_i\left(R + R_f\right) + RR_f\right]}{R_i\left(R + R_f + KR\right) + RR_f + R_o\left(R + R_i\right)}$$ (50)

Calculating $\left(R_{oF}\right)_1 = \lim_{R_i \to \infty} R_{oF}$ we have,

$$\left(R_{oF}\right)_1 = \frac{R_o\left(R + R_f\right)}{R + R_f + KR + R_o}$$ (51)

finally, $R_o + R + R_f + KR \ \Box \ R + R_f + KR$, the ideal output resistance $\left(R_{oF}\right)_i$ of the noninverting amplifier is given by,

$$\left(R_{oF}\right)_i = \frac{R_o}{1 + \dfrac{KR}{R + R_f}} \tag{52}$$

This result shows that the ideal output resistance of the noninverting amplifier is $\dfrac{1}{\left(1 + KR/R + R_f\right)}$ times the output resistance R_o of the op-amp. That is , the output resistance of the op-amp with feedback is much smaller than the output resistance without feedback. In addition (52) can be verified in (Stanley, 1994; Gayakward, 2000).

6.1.3 Bandwidth of the noninverting amplifier

The bandwidth of an amplifier is defined as the band (range) of frequency for which the gain remains constant. Manufacturers generally specify either the gain-bandwidth product or supply open loop gain versus frequency curve for the op-amp (Gayakward, 2000).

Fig. 4 shows the open loop gain versus frequency curve of the $\mu A741$ op-amp. From this curve for a gain of 200,000, the bandwidth is approximately $5Hz$; or the gain-bandwidth product is $1MHz$. On the other extreme, the bandwidth is approximately $1MHz$ when the gain is 1. Hence, the frequency at which the gain equals 1 is known as the unity gain bandwidth (UGB).

Since for an op-amp with a single break frequency f_o, the gain-bandwidth product is constant, and equal to UGB, we can write,

$$UGB = \left(K\right)\left(f_o\right) = \left(A_{CL}\right)\left(f_F\right) \tag{53}$$

where f_F bandwidth with feedback.

Therefore, the bandwidth of an feedback op-amp is,

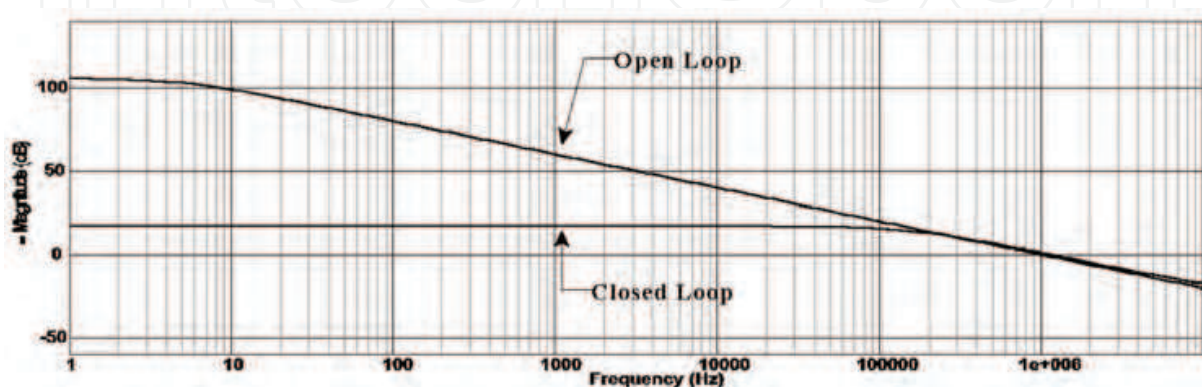$$f_F = \frac{(K)(f_o)}{A_{CL}} \tag{54}$$

Fig. 14. Frequency response of the noninverting amplifier.

The frequency response of the noninverting amplifier based on BGI of Fig. 11, using $\mu A741$ op-amp, $R = 1K\Omega$, $R_f = 5K\Omega$ and the input signal is $v_i(t) = 1.0\sin(2\pi f_i t)V$ where $f_i = 30KHz$, is shown in Fig. 14.

Note that the frequency response of this amplifier indicates that the closed loop gain is $A_{CL} = 6 = 15.56dB$ until approximately $166KHz$, which is verified from (54).

6.1.4 Slew rate

Another important frequency related parameter of an op-amp is the slew rate. The slew rate is the maximum rate of change of output voltage with respect to time, usually specified in $V/\mu s$. Ideally, we would like an infinity slew rate so that the op-amp's output voltage would change simultaneously with the input. Practical op-amps are available with slew rates from $0.1V/\mu s$ to well above $1000V/\mu s$. The slew rate (SR) can be obtained by,

$$SR = \frac{2\pi f V_p}{10^6} V/\mu s \qquad (55)$$

where f is the input frequency and V_p is the peak value of the output sine wave.

In order to show the effect of the slew rate of an op-amp, the time responses of the noninverting amplifier based on BGI of Fig. 11, using $\mu A741$ and $OP27$ op-amps, $R = 1K\Omega$, $R_f = 5K\Omega$ and the input signal is $v_i(t) = 1.0\sin(2\pi f_i t)V$ where $f_i = 30KHz$, are shown in Fig. 15. The ideal closed gain is then $(A_{CL})_i = 6$.
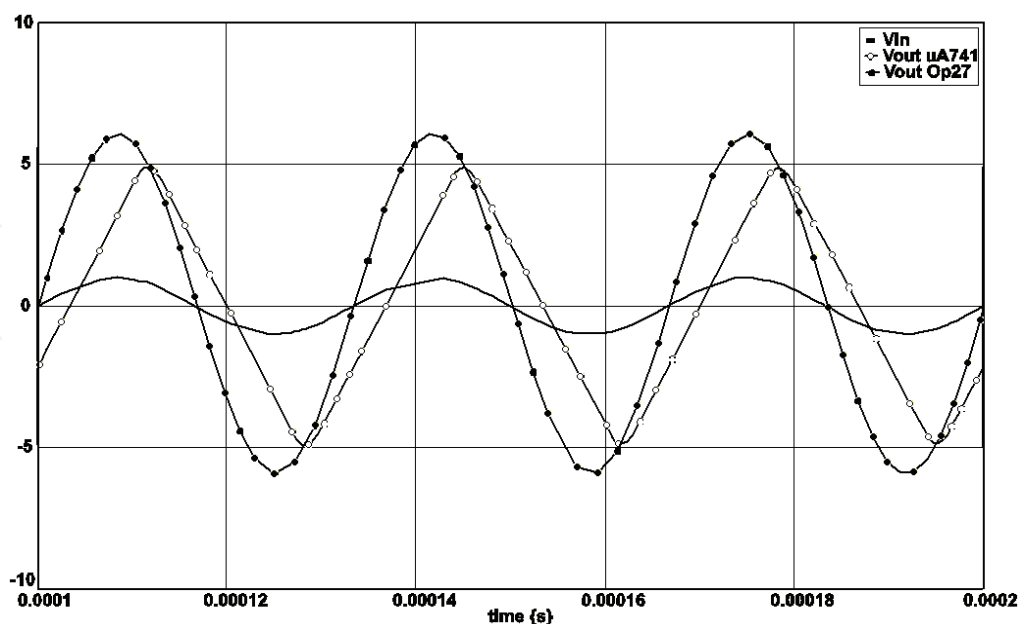

Fig.15. Effect of the slew rate of the noninverting amplifier using $\mu A741$ and $OP27$ op-amps.

From (55), the minimum slew rate of an op-amp with the previous conditions is $SR = 1.13 \, V/\mu s$. Therefore, the slew rate of the $OP27$ op-amp, which is $2.8 \, V/\mu s$ is enough for the input signal with the given conditions. Fig. 15, shows the output signal of the $\mu A741$ op-amp has distortion because of the slew rate is $0.5 \, V/\mu s$.

6.1.5 Supply volages

The most linear integrated circuits, particularly op-amps, use one or more differential amplifier stages, and differential amplifiers require both a positive (V_c) and negative (V_e) power supply for proper operation of the circuit.

The supply voltages of the proposed bond graph model of an op-amp can be tested applying an input signal $v_i(t) = 3\sin(2\pi f_i)t$, $f_i = 30KHz$, $R = 1K\Omega$, $R_f = 5K\Omega$ and $V_c = 12V$ and $V_e = -12V$ to $\mu A741$ op-amp, the time response is shown in Fig. 16.

The ideal closed loop gain is $(A_{CL})_i = 6$, of this form the ideal output signal would be $V_{out}(t) = 18\sin(2\pi f_i)t$. However, the supply voltages of the op-amp are $\pm 12V$, limiting the output signal to this rank of voltage.

Next section, the op-amp integrator that is one the most interesting configurations on a bond graph model is designed.
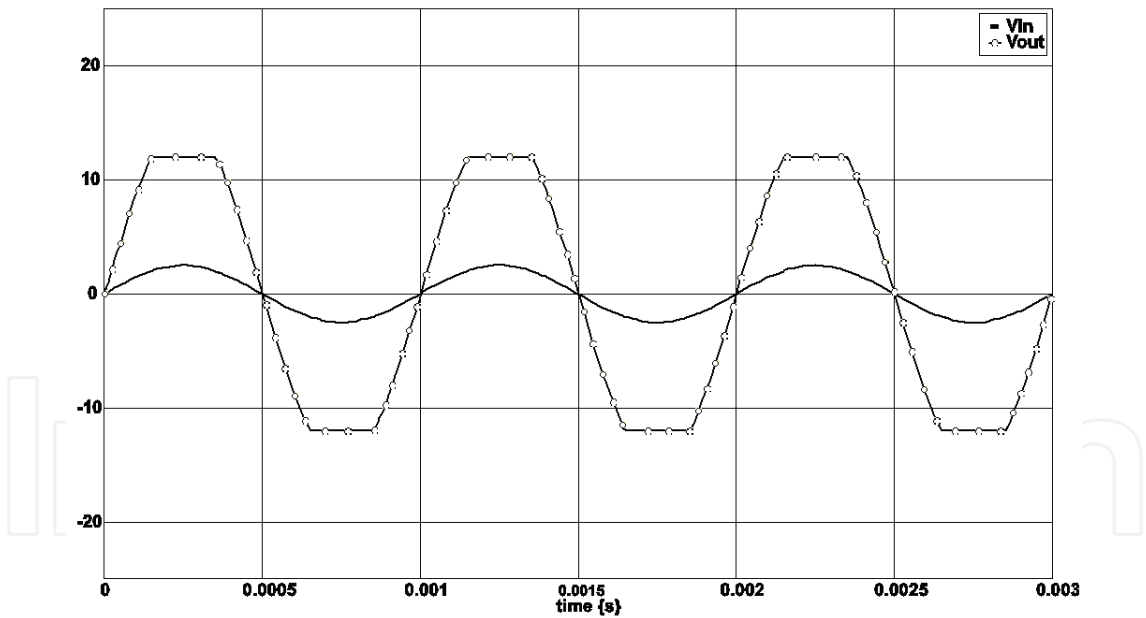
Fig.16. Time response with slew rate and supply voltages using $\mu A741$ op-amp.

6.2 The operational amplifier integrator

An op-amp integrator simulates mathematical integration, which is basically a summing process that determines the total area under the curve of a function (Floyd & Buchla, 1999). A basic integrator on a BGD model is shown in Fig. 17. Notice that the feedback element is a capacitor that forms an RC circuit with the input.

Fig. 17. Bond graphs of an operational amplifier integrator.

In order to determine the transfer function of the op-amp integrator based on bond graph model of Fig. 17, the methodology given in Section 1 is applied. The key vectors are,

$$x(t) = \begin{bmatrix} q_{11}(t) \\ q_{18}(t) \end{bmatrix}; \dot{x}(t) = \begin{bmatrix} f_{11}(t) \\ f_{18}(t) \end{bmatrix}; z(t) = \begin{bmatrix} e_{11}(t) \\ e_{18}(t) \end{bmatrix}; \begin{matrix} u(t) = e_1(t) \\ y(t) = e_9(t) \end{matrix}$$

$$D_{in}(t) = \begin{bmatrix} e_4(t) & e_7(t) & e_9(t) & f_{13}(t) & e_{15}(t) \end{bmatrix}^T \tag{56}$$

$$D_{out}(t) = \begin{bmatrix} f_4(t) & f_7(t) & f_9(t) & e_{13}(t) & f_{15}(t) \end{bmatrix}^T$$

the constitutive relations are,

$$F = diag\left\{ \frac{1}{C}, \frac{1}{C_h} \right\} \tag{57}$$

$$L = diag\left\{ \frac{1}{R_i}, \frac{1}{R_o}, \frac{1}{R_L}, R, \frac{1}{R_h} \right\} \tag{58}$$

and the junction structure matrix is,

$$S_{22} = \begin{bmatrix} 0 & 0 & 0 & 1 & 0 \\ 0 & 0 & 0 & m_2 & 0 \\ 0 & 0 & 0 & -1 & 0 \\ -1 & -m_2 & 1 & 0 & 0 \\ 0 & 0 & 0 & K & 0 \end{bmatrix}; S_{23} = \begin{bmatrix} -1 \\ -m_2 \\ 1 \\ 0 \\ -K \end{bmatrix}; S_{21} = \begin{bmatrix} 0 & 0 \\ m_2 & 1 \\ -1 & 0 \\ 0 & 0 \\ 0 & -m_2 \end{bmatrix} \tag{59}$$

$$S_{12} = \begin{bmatrix} 0 & -m & 1 & 0 & 0 \\ 0 & 0 & 0 & 0 & m_1 \end{bmatrix}; \begin{matrix} S_{32} = \begin{bmatrix} 0 & 0 & 0 & -1 & 0 \end{bmatrix}; S_{33} = 1 \\ S_{31} = \begin{bmatrix} -1 & 0 \end{bmatrix}; S_{11} = S_{13} = 0 \end{matrix}$$

From (8), (13), (57), (58) and (59) the A_p matrix is,

$$A_p = \begin{bmatrix} \dfrac{-1}{C}\left(R_o + m_2^2 R_L\right)\left(R + R_i\right) & \dfrac{-1}{C_h}\left(R + R_i\right)m_2 R_L \\[3mm] \dfrac{-1}{C}\left(R_o + m_2^2 R_L\right)m_1 KRR_i & \dfrac{-m_1}{C_h R_h}\left(\Delta + m_2 KRR_i R_L\right) \end{bmatrix} \tag{60}$$

where $\Delta = R_o\left[R_L\left(R + R_i\right) + RR_i\right] + m_2^2 RR_L R_i$

Substituting (13), (58) (59) into (9), B_p is determined by,

$$B_p = \frac{1}{\Delta}\begin{bmatrix} R_i\left(R_o + m_2^2 R_L\right) \\[3mm] \dfrac{-1}{R_h}\left(m_1 KR_o R_i R_L\right) \end{bmatrix} \tag{61}$$

From (10), (13), (57), (58) and (59) the C_p matrix is,

$$C_p = \frac{1}{\Delta}\begin{bmatrix} \dfrac{-1}{C}\left(R + R_i\right)R_o R_L & \dfrac{1}{C_h}m_2 RR_i R_L \end{bmatrix} \tag{62}$$

Finally, substituting (13), (58) and (59) into (11), D_p is given by,

$$D_p = \frac{1}{\Delta}R_o R_i R_L \tag{63}$$

The transfer function of a system represented in space state can be calculated by,

$$G(s) = C_p\left(sI_n - A_p\right)^{-1}B_p + D_p \tag{64}$$

Substituting (60), (61), (62) and (63) into (64), the transfer function of the op-amp integrator of Fig. 17 is,

$$G(s) = \frac{\left(s^2 CC_h R_h R_o + sCR_o m_1^2 - Km_1 m_2\right)R_L R_i}{s^2 CC_h R_h \Delta + s\left(C_h R_h \Delta + CRR_L R_i Km_1 m_2 + Cm_1^2 \Delta\right) + m_1^2 \Lambda} \tag{65}$$

where $\Lambda = \left(R + R_i\right)\left(R_o + m_2^2 R_L\right)$.

Considering a normal operation of the op-amp, $m_1 = m_2 = 1$ and $R_o = 0$, we have,

$$G_1(s) = \frac{-1}{s^2\,\dfrac{CC_h R_h R}{K} + s\left[\dfrac{C_h R_h}{K}\left(\dfrac{R}{R_i} + 1\right) + CR + \dfrac{CR}{K}\right] + \dfrac{1}{K}\left(\dfrac{R}{R_i} + 1\right)} \tag{66}$$

In addition, applying $\lim_{\substack{R_i \to \infty \\ K \to \infty}} G_1(s)$, the ideal transfer function, $G_i(s)$, is determined by,

$$G_i(s) = \frac{-1}{sRC} \tag{67}$$

Note that, (67) is the typical transfer function of a integral controller. However, the equation (65) is the transfer function of a integral controller based on op-amp and considering their internal parameters and external elements.

The time response of the integrator circuit using $\mu A741$ op-amp and $R = 10\Omega$, $C = 100\mu F$ and $v_i(t) = \sin(2\pi f_i t)V$ where $f_i = 1KHz$ shows in Fig. 18. The output signal proves that the bond graph model of Fig. 18, is an integrator of the input signal.
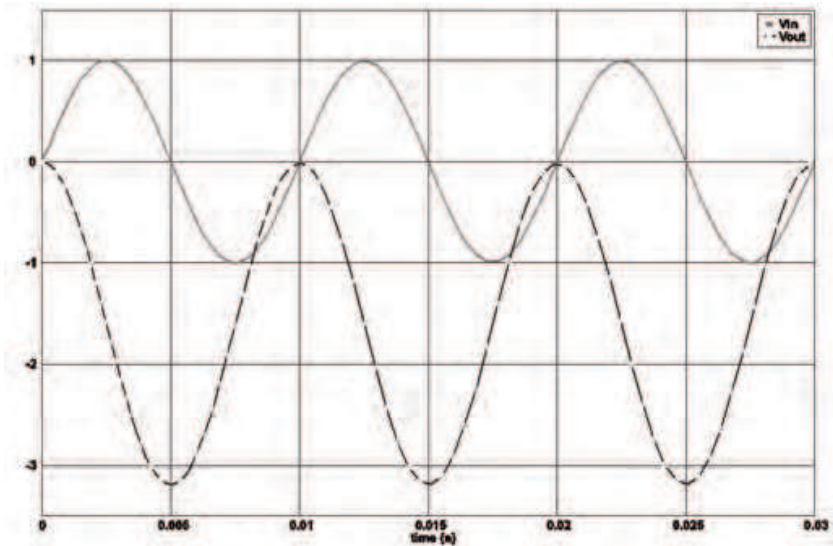
Fig. 18. Time response of the integrator.

The frequency response of the integrator circuit of Fig. 17 is shown in Fig. 19. Note that (67) is represented by Fig. 19.
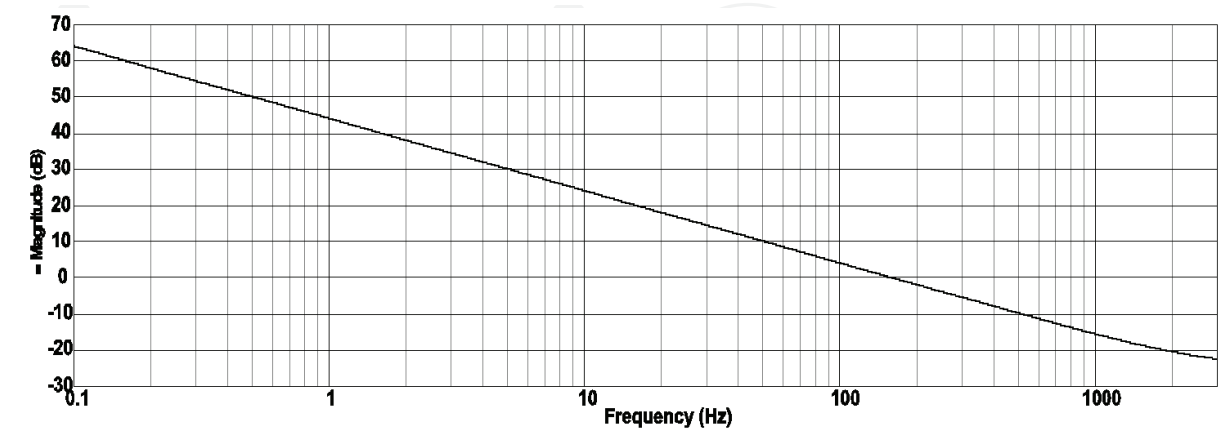

Fig. 19. Frequency response of the integrator circuit.

Next section an important application of the op-amp that is an active filter in the physical domain is proposed.

7. Active filters using bond graph models

An electric filter is often a frequency selective circuit that passes a specified band of frequencies and blocks or attenuates signals of frequencies outside this band. Filters may be classified in a number of ways (Gayakward, 2000):

1. Analog or digital. Analog filters are designed to process analog signals, while digital filters process analog signals using digital techniques.
2. Passive or active. Passive filters use resistors, capacitors and inductors in their construction and the active filters employ transistor or op-amps in addition to resistors and capacitors.

An active filter offers the following advantages over a passive filter: a) Gain and frequency adjustment flexibility. b) No loading problem. c) Cost.

A filter will usually conform to one of four basic response types: low-pass, high-pass, band-pass and band-reject.

7.1 Low-pass filter

A low-pass filter allows only low frequency signals to pass through, while suppressing high-frequency components. The bond graph model of a low-pass filter is shown in Fig. 20.

Fig. 20. Bond graph model of a low-pass filter.

The key vectors of the bond graph of Fig. 20 are,

$$x(t) = \begin{bmatrix} q_{17}(t) \\ q_{23}(t) \end{bmatrix}; \dot{x}(t) = \begin{bmatrix} f_{17}(t) \\ f_{23}(t) \end{bmatrix}; z(t) = \begin{bmatrix} e_{17}(t) \\ e_{23}(t) \end{bmatrix}; \begin{matrix} u(t) = e_1(t) \\ y(t) = e_9(t) \end{matrix}$$

$$D_{in}(t) = \begin{bmatrix} e_4(t) & e_7(t) & e_9(t) & f_{11}(t) & f_{13}(t) & e_{14}(t) & e_{21}(t) \end{bmatrix}^T \qquad (68)$$

$$D_{out}(t) = \begin{bmatrix} f_4(t) & f_7(t) & f_9(t) & e_{11}(t) & e_{13}(t) & f_{14}(t) & f_{21}(t) \end{bmatrix}^T$$

The constitutive relations of the elements are,

$$F = diag\left\{ \frac{1}{C_h}, \frac{1}{C_e} \right\} \qquad (69)$$

$$L = diag\left\{\frac{1}{R_i},\frac{1}{R_o},\frac{1}{R_L},R_f,R,\frac{1}{R_h},\frac{1}{R_c}\right\} \tag{70}$$

and the junction structure is

$$S_{22} = \begin{bmatrix} 0_{3\times3} & P_1 \\ -P_1^T & 0_{2\times2} & 0_{7\times2} \\ 0_{2\times3} & P_2 \end{bmatrix}; S_{21} = \begin{bmatrix} 0 & 1 \\ 1 & 0 \\ 0_{3\times2} \\ -m_1 & K \\ 0 & -1 \end{bmatrix}$$

$$S_{12} = \begin{bmatrix} 0 & m_1 & 0 \\ -1 & 0_{2\times4} & 0 & 1 \end{bmatrix}; S_{23} = \begin{bmatrix} 0_{6\times1} \\ 1 \end{bmatrix} \tag{71}$$

$$S_{32} = \begin{bmatrix} 0_{1\times3} & -1 & 1 & 0_{1\times2} \end{bmatrix}; S_{11} = S_{13} = S_{31} = S_{33} = 0$$

where

$$P_1 = \begin{bmatrix} 0 & -1 \\ m_2 & -m_2 \\ -1 & 1 \end{bmatrix}; P_2 = \begin{bmatrix} 0 & -K \\ 0 & 0 \end{bmatrix} \tag{72}$$

From (8), (13), (69), (70) and (71), the A_p matrix of the low-pass filter is,

$$A_p = \begin{bmatrix} \dfrac{-m_1^2}{R_h C_h} - \dfrac{m_1 m_2 KRR_L R_i}{\Delta C_h} & \dfrac{-m_1 K}{R_h C_h} - \dfrac{m_1 RK}{\Delta C_h}\left[R_o\left(R_L + R_f\right) + m_2^2 R_L R_f\right] \\ \dfrac{m_2 RR_L}{\Delta C_h} & \dfrac{-1}{R_c C_c} - \dfrac{1}{\Delta C_h}\left[\left(R + R_f\right)\left(R_o + m_2^2 R_L\right) + R_o R_L\right] \end{bmatrix} \tag{73}$$

where $\Delta = R_o\left[\left(R_L + R_f\right)\left(R + R_i\right) + RR_i\right] + m_2^2\left[RR_L\left(R_f + R_i\right) + R_L R_f R_i\right]$

Substituting (70) and (71) into (13), the B_p matrix is obtained

$$B_p = \begin{bmatrix} 0 & \dfrac{1}{R_c} \end{bmatrix}^T \tag{74}$$

Finally, from (10), (13), (69), (70) and (71), the C_p matrix is

$$C_p = \left[\frac{m_2 R_L}{\Delta C_h} \left[R\left(R_i + R_f \right) + R_i R_f \right] \quad \frac{R R_L R_o}{\Delta C_h} \right]$$ (75)

and $D_p = 0$

From (73) to (75), and (64), and considering ideal characteristics of the op-amp, $R_o = 0$, $R_i = \infty$, $K = \infty$ and $R_L = \infty$, the ideal transfer function of the low-pass filter, denoted by $G_i(s)$ is obtained $G_i(s) = \dfrac{A_{CL}/R_c C_c}{s + 1/R_c C_c}$ where $A_{CL} = 1 + \dfrac{R_f}{R}$.

The ideal transfer function of the low-pass filter indicates that on the pass band the gain is almost A_{CL} and the pole of the system is located at the high cutoff frequency f_h defined by $f_h = \dfrac{1}{2\pi C_c R_c}$.

The frequency response of the low-pass filter based on bond graph model using the μA741 op-amp and considering the numerical values of the Table 3 is shown in Fig 21.

R	R_f	R_L	R_c	C_C
$10K\Omega$	$10K\Omega$	$1K\Omega$	$15.9K\Omega$	$1 \times 10^{-8} F$

Table 3. Numerical values of the low-pass filter.
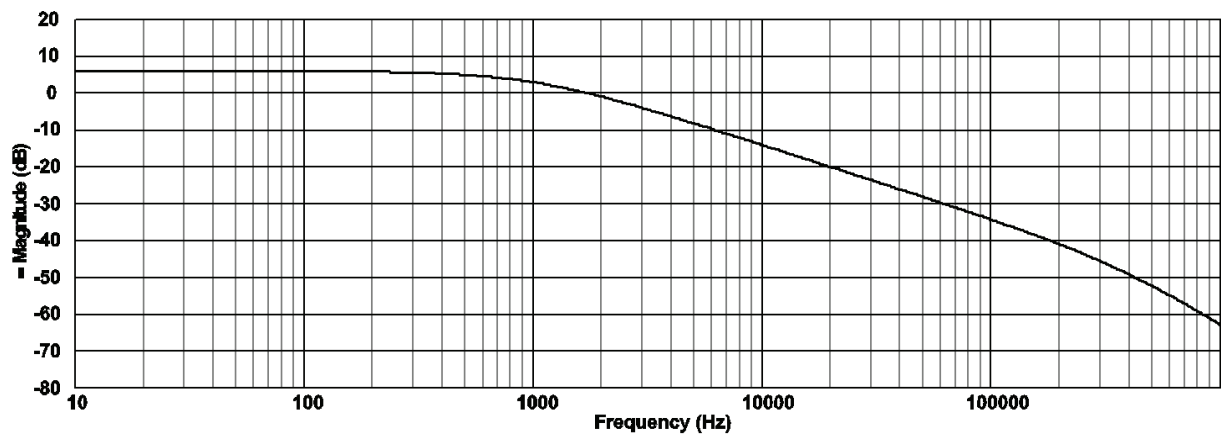
Fig. 21. Frequency response of the low-pass filter.

The Fig 21 shows that $f_h = 1KHz$. Also, we have a first order filter, because the filter has a pole and the rolloff rate of the filter is 20 dB per decade.

7.2 High-pass filter

A high pass filter allows only frequencies above a certain break point to pass through. In other words, it attenuates low frequency components. A first order high-pass filter on bond graph model is shown in Fig. 22.
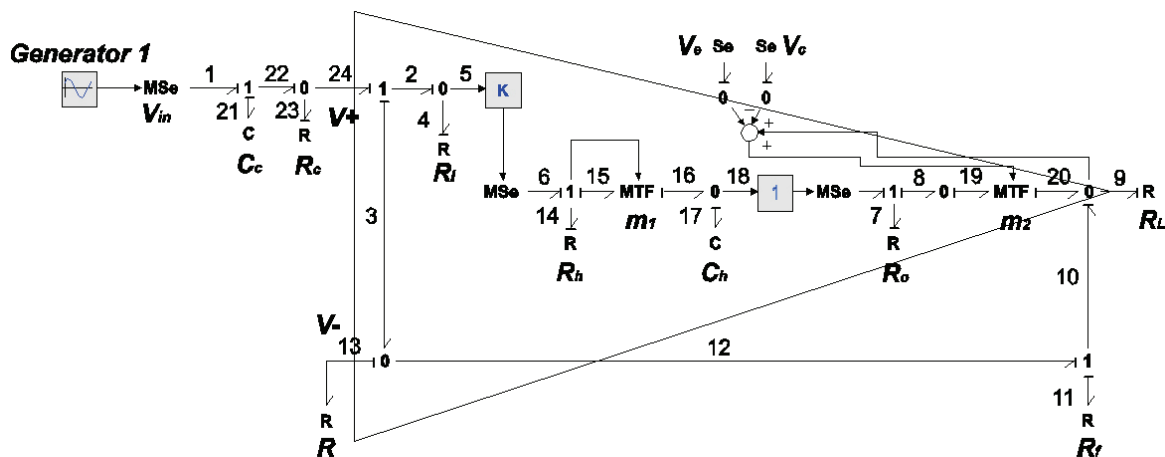
Fig. 22. Bond graph model of a high-pass filter.

The mathematical model of the filter can be determined in the same manner that the low-pass filter. However, for all the remaining filters of this paper, we use the software 20-sim to know the performance of the filter on the physical domain, considering the internal characteristics of the op-amp and the external components connected to the op-amp in order to get the filter type.

Using the same numerical values that the low-pass filter, the frequency response of the filter shows in Fig. 23.
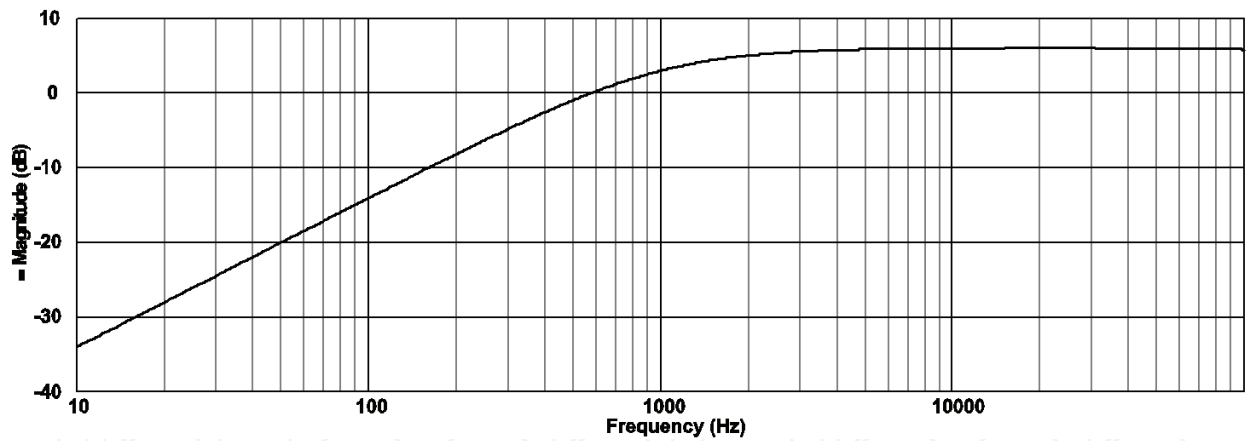
Fig. 23. Frequency response of the high-pass filter.

The Fig. 23 indicates that we have a first order filter and the low cutoff frequency f_L is $1KHz$.

7.3 Band-pass filter

The band-pass filter can be thought of as a combination of high and low pass filters. It allows only frequencies within a specified rang to pass through. In Fig. 24 a band-pass filter on bond graph model is proposed. The characteristic of this filter is a narrow band-pass using multiple feedback .

In order to get the performance of this filter, we use the internal parameters of the $\mu A741$ op-amp given in Tables 1 and 2, and the external components are shown in Table 4.
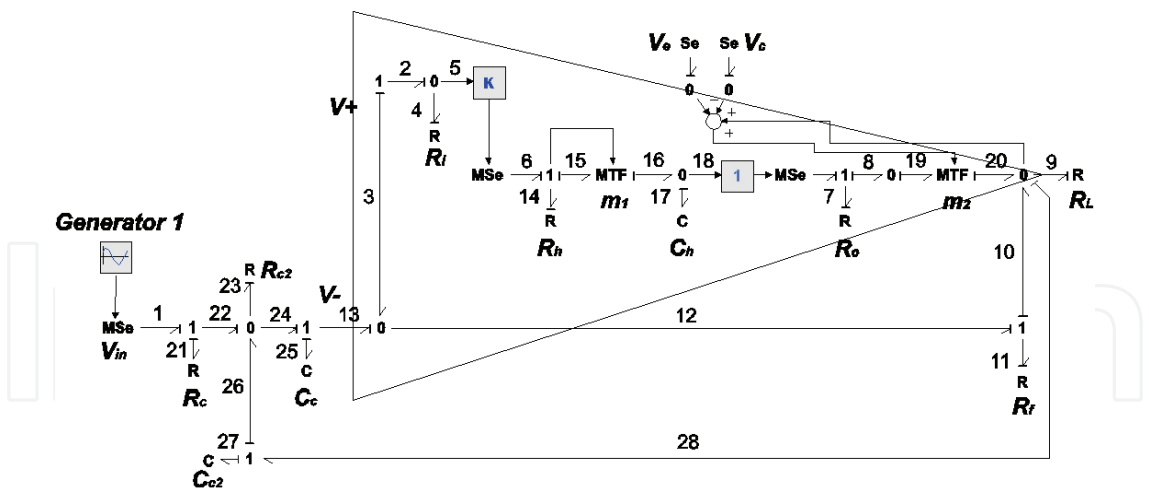
Fig. 24. Bond graph model of a band-pass filter.

R_c	R_f	R_L	R_{c2}	C_c	C_{c2}
$4.77K\Omega$	$100K\Omega$	$10K\Omega$	$0.2K\Omega$	$0.01\mu F$	$0.01\mu F$

Table 4. Numerical values of the external components

The frequency response of the band-pass filter is shown in Fig. 25.
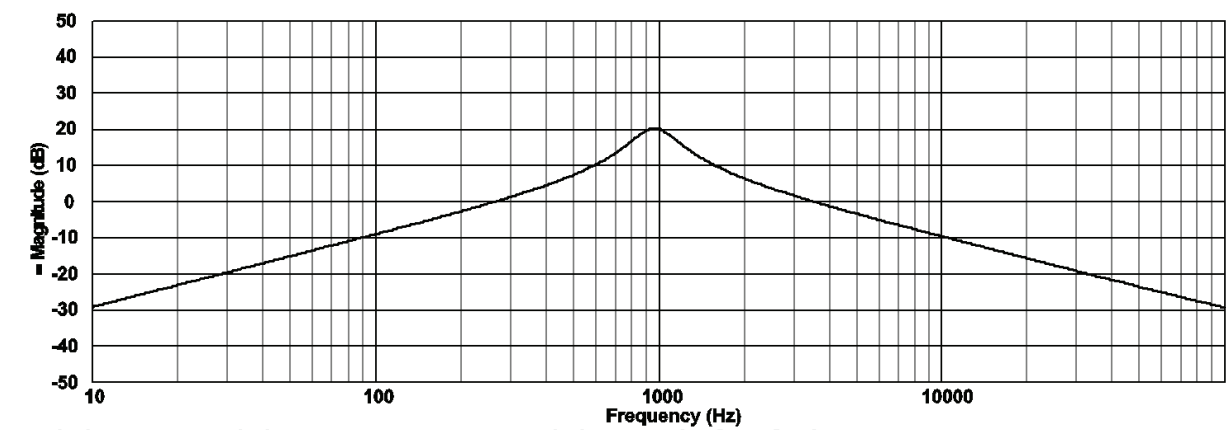
Fig. 25. Frequency response of the band-pass filter.

Note that, the response of the filter allows to pass the frequency component of $1KHz$ with a closed loop gain of 10 and the low and high frequencies respect to $1KHz$ have a small magnitude.

7.4 Band-reject filter

The band-reject filter allows everything to pass through with the exception of a specific range of frequencies. The band-reject filter is often called notch filter, because it is commonly used for the rejection of a single frequency. The Fig. 26 shows this filter on a bond graph model.

Using the parameters of the $\mu A741$ op-amp given on Tables 1 and 2, and the external elements of the op-amp of Fig. 26 are gotten in Table 5, the frequency response of the filter is shown in Fig. 27.
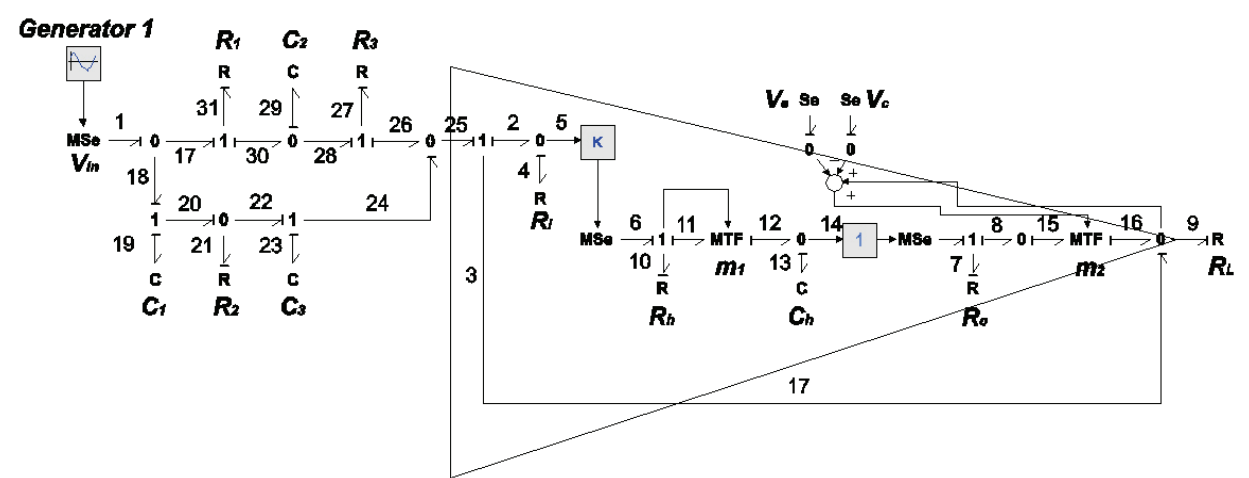
Fig. 26. Bond graph model of a band-reject filter.

R_1	R_2	R_3	R_L	$C_1 = C_3$	C_2
$39K\Omega$	$19.5K\Omega$	$39K\Omega$	$1K\Omega$	$0.068\mu F$	$0.136\mu F$

Table 5. External elements of the band-reject filter.
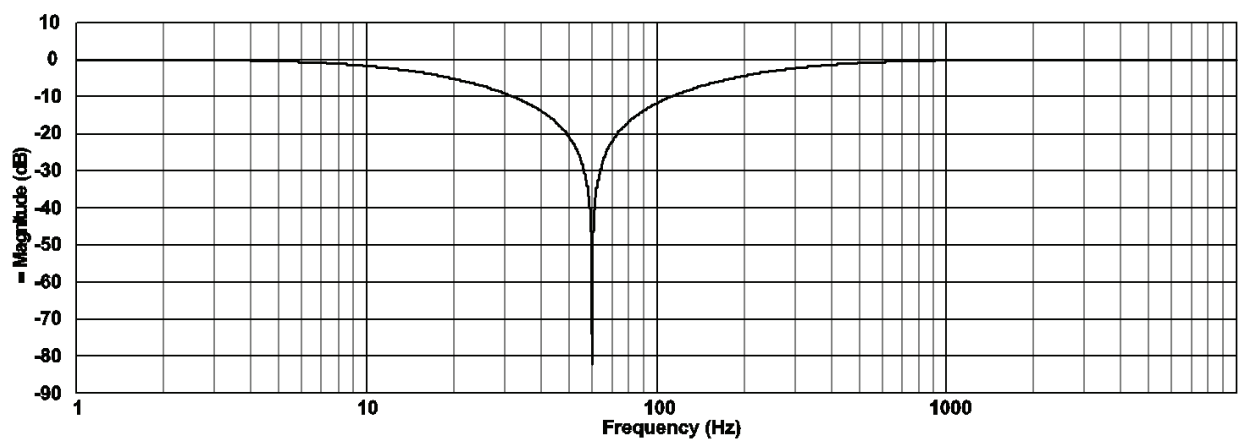
Fig. 27. Frequency response of the band-reject filter.

In Fig. 27, we show that $60Hz$ power line frequency can be attenuated using this filter in the physical domain.

7.5 Applying active filters

A filter is a circuit which inhibits the transfer of a specific range of frequencies. So, we can apply active filters to select a frequency component of a complex signal. An interesting application of filters on bond graph models is shown in Fig. 28 where we have an input signal given by,

$$V_i = 0.1\sin\left[2\pi\left(10Hz\right)t\right] + 0.1\sin\left[2\pi\left(500Hz\right)t\right] + 0.1\sin\left[2\pi\left(20KHz\right)t\right] \quad (76)$$

In Fig. 28, the input is applied to low-pass filter denoted by opamp1, to high-pass filter denoted by opamp2 and to band-pass filter denoted by opamp3.

Also, the external elements of Fig. 28 are obtained on Table 6 and using the parameters of the $\mu A741$ op-amp given on Tables 1 and 2, the frequency responses are shown in Fig. 29.
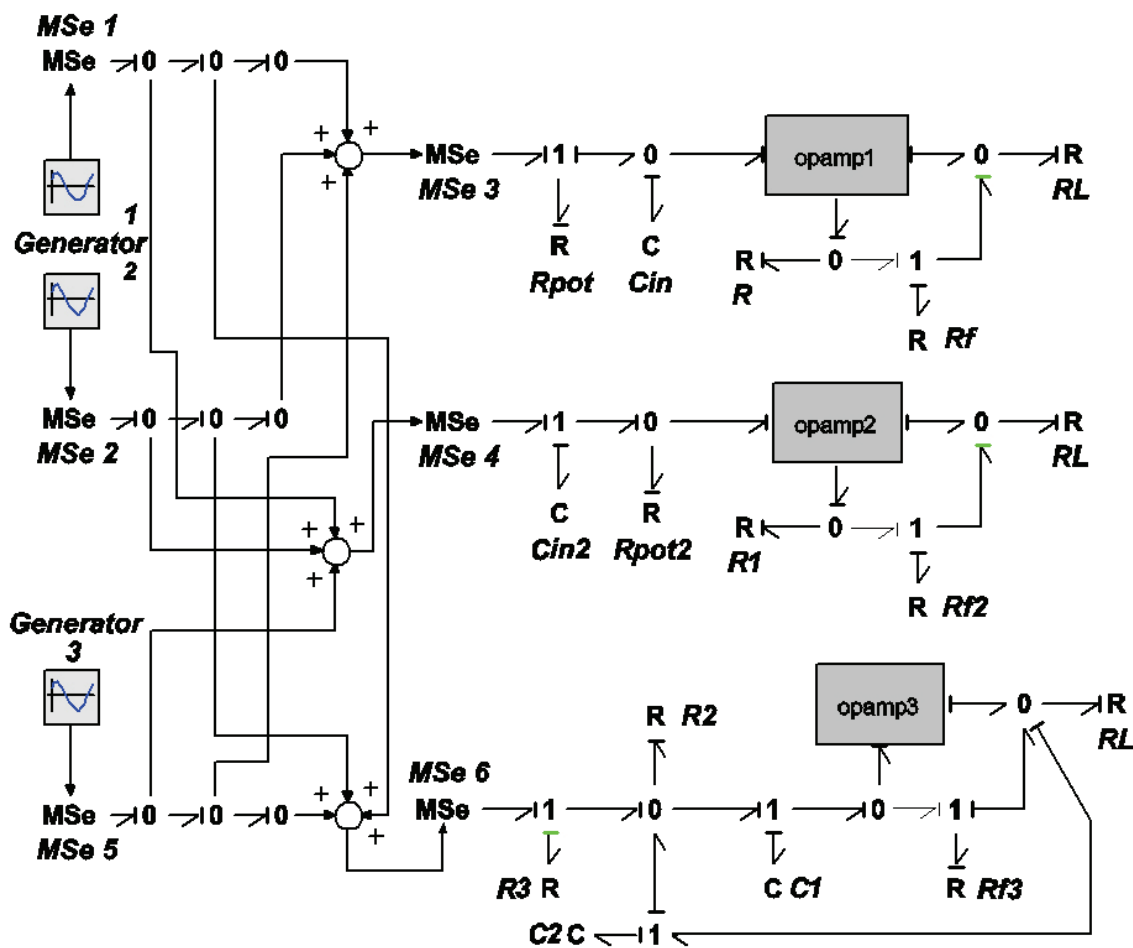
Fig. 28. Compose signal applied to bond graph filters.

$R = R_1$	$R_f = R_{f2}$	C_{in}	R_{pot}
$1M\Omega$	1Ω	$1\mu F$	$15.9K\Omega$
R_3	R_{f3}	$C_1 = C_4 = C_{in2}$	R_2
$95.5K\Omega$	$191K\Omega$	$0.01\mu F$	$5.6K\Omega$

Table 6. External elements of the compose system.

In Fig. 29, the high cutoff frequency is $f_H = 10Hz$ for the low-pass filter, the low cutoff frequency is $f_L = 20KHz$ for the high-pass filter and the center frequency is $f_c = 500Hz$.

Finally, the time response of each filter is shown in Fig. 30 and we note that the objective of the filters is successful.
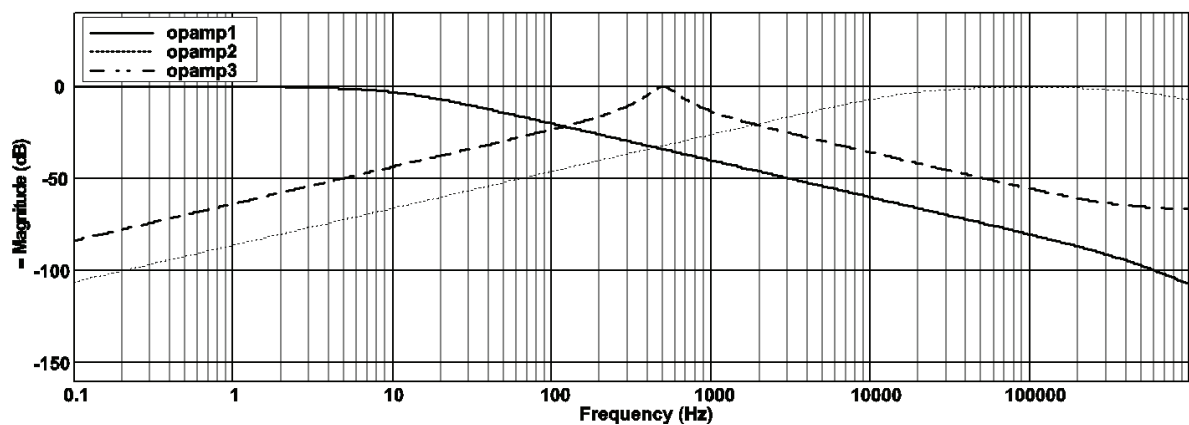
Fig. 29. Frequency response of a complete system.
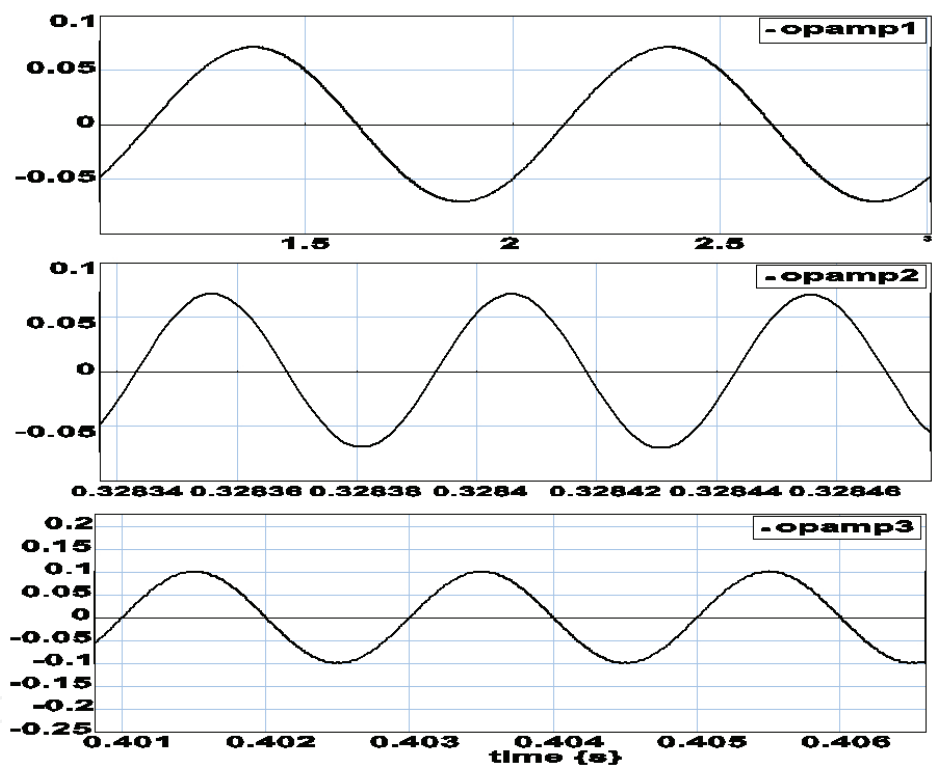
Fig. 30. Time response of the complete system.

Note that the bond graph model of the op-amp to design controllers, analog computers and general linear applications can be applied.

8. Controller based on bond graph model of an operational amplifier

Another important application of operational amplifiers is to implement controllers and can be used to improve the performance of a closed loop system. A proportional and integral (PI) controller designed in the physical domain to control the velocity of a DC motor is applied (Barna & Porat, 1989).

The noninverting and integrator configurations of an op-amp are used to derive the PI controller. Also, the input reference of the system is voltage V_n and on the feedback a element GY to connect the output with the summing junction is applied. The BGI of the closed loop system is shown in Fig. 31.
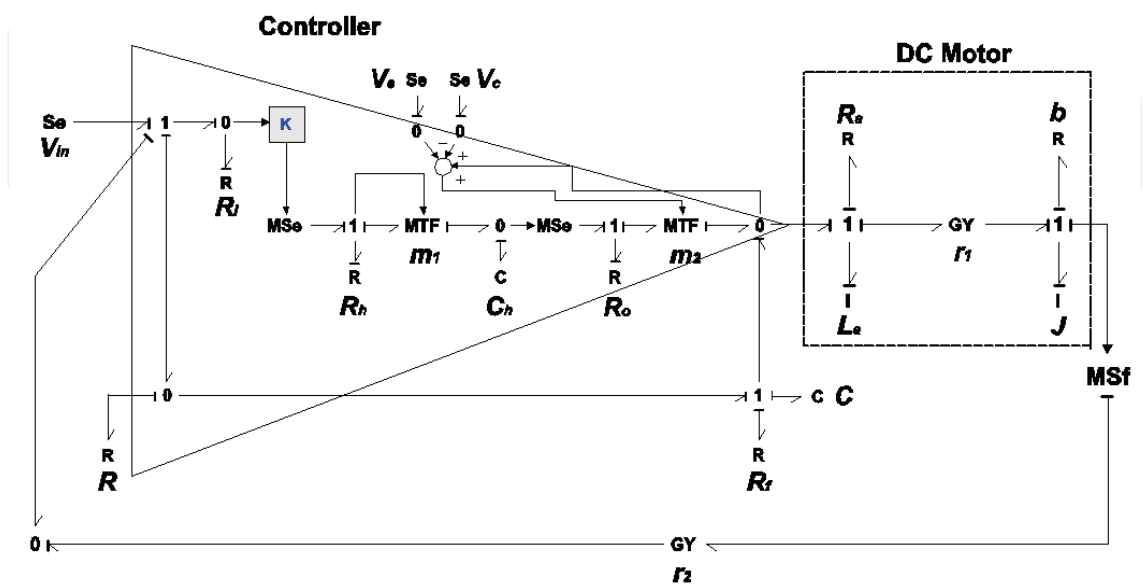
Fig. 31. PI Controller of DC motor on a bond graph model.

The BGI of Fig. 31 can be used to determine the state space representation or the transfer function of the closed loop system. However, in this case we only show the simulation with the objective to test the PI controller connected to DC motor in a closed loop system.
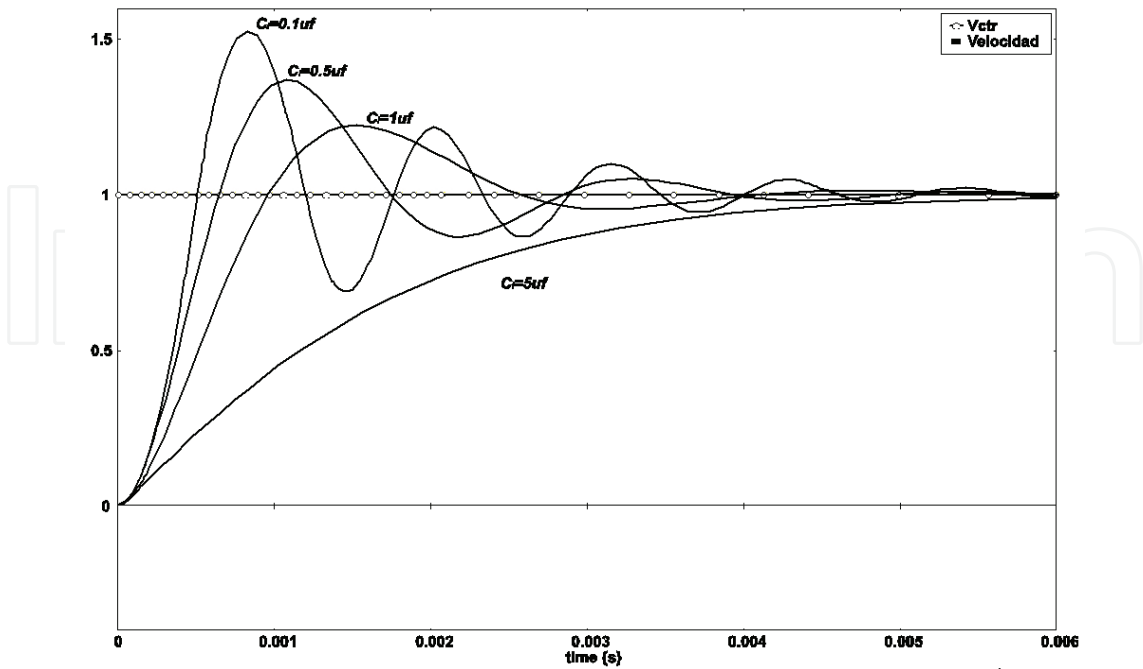
Fig. 32. Time response of the output of the DC motor using a PI controller.

The time response of the output using a $\mu A741$ op-amp, $R = 10K\Omega$, $R_f = 90K\Omega$, $R_a = 2\Omega$, $L_a = 0.01mH$, $J = 0.001Kgm^2$ and $b = 1Nm/rad/s$, is shown in Fig. 32. Note that the PI Controller yields a steady state output equal to input reference of the system and the transient response depends of the parameters of the system and controller.

9. Conclusions

In this work an operational amplifier is shown in a bond graph model. The proposed bond graph takes account the input and output resistances, open loop gain, supply voltages, slew rate and frequency compensation of an operational amplifier. Therefore, an advantage of this model is to determine the performance of applications based on operational amplifiers considering the type of linear integrated circuit to obtain the internal parameters from the data sheets. Finally, open loop and closed loop configurations of the operational amplifier in the physical domain have been shown.

10. References

Arpad Barna and Dan I. Porat, (1989). *Operational Amplifiers*, John Wiley & Sons,ISBN:0-471-63764-5, Canada

C. Sueur, G. Dauphin-Tanguy, (1991), Bond graph approach for structural analysis of MIMO linear systems, *Journal of the Franklin Institute*, vol. 328, no.1 , (55-70).

Dean C. Karnopp, Ronald C. Rosenberg, (1975). *System Dynamics: A Unified Approach*, Wiley, John & Sons,

Forbes T. Brown (2001)., *Engineering System Dynamics*, Marcel Dekker Inc, ISBN:0-8247-0616-1, United States of America.

Gilberto Gonzalez, Dauphin- Tanguy G. Galindo R and De Leon J. (2005), Steady State Error for a Closed Loop Physical System with a Bond Graph Approach, *Proceedings of International Conference on Bond Graph Modeling and Simulation*, pp. 107-112, ISBN:1-56555-287-3, New Orleans, January 2005, SCS.

Norman S. Nise, (2000). *Control Systems Engineering*, John Wiley & Sons, ISBN:970-24-0254-9, United States of America.

Peter Gawthrop, Lorcan Smith (1996)., *Metamodelling*, Prentice-Hall,ISBN:0-13-489824-9, Great Britain.

P.E. Wellstead, (1979). *Physical System Modelling*, Academic Press, ISBN:0-12-744380-0 London.

P. J. Gawthrop and D. Palmer, (2003). A bicausal bond graph representation of operational amplifiers", *Proceedings of the Institution of Mechanical Engineers Part I: Journal Systems and Control Engineering*, Vol. 217

Ramakant A. Gayakward, (2000), *Op-amps and Linear Integrated Circuit*, Prentice Hall, ISBN:0-13-280868-4, United States of America.

Thomas L. Floyd and David Buchla, (1999), *Basic Operational Amplifiers and Linear Integrated Circuits*, Prentice-Hall, ISBN:0-13-082987-0, United States of America.

William D. Stanley, (1994). *Operational Amplifiers with Linear Integrated Circuits*, Maxwell Macmillan International

20-Sim, Controllab Products (2007) B. V., 20-Sim, *http://www.20sim.com/ product/20sim.html*

New Approaches in Automation and Robotics

Edited by Harald Aschemann

The book New Approaches in Automation and Robotics offers in 22 chapters a collection of recent developments in automation, robotics as well as control theory. It is dedicated to researchers in science and industry, students, and practicing engineers, who wish to update and enhance their knowledge on modern methods and innovative applications. The authors and editor of this book wish to motivate people, especially under-graduate students, to get involved with the interesting field of robotics and mechatronics. We hope that the ideas and concepts presented in this book are useful for your own work and could contribute to problem solving in similar applications as well. It is clear, however, that the wide area of automation and robotics can only be highlighted at several spots but not completely covered by a single book.

How to reference

In order to correctly reference this scholarly work, feel free to copy and paste the following:

Gilberto Gonzalez and Roberto Tapia (2008). Operational Amplifiers and Active Filters: A Bond Graph Approach, New Approaches in Automation and Robotics, Harald Aschemann (Ed.), ISBN: 978-3-902613-26-4, InTech, Available from:

http://www.intechopen.com/books/new_approaches_in_automation_and_robotics/operational_amplifiers_and_active_filters__a_bond_graph_approach

INTECH
open science | open minds